THE JOURNAL OF BIOLOGICAL CHEMISTRY Vol. 277, No. 30, Issue of July 26, pp. 27553–27558, 2002
Printed in U.S.A.

Structural Basis of Thermostability

ANALYSIS OF STABILIZING MUTATIONS IN SUBTILISIN BPN′*

Received for publication, December 10, 2001, and in revised form, April 30, 2002
Published, JBC Papers in Press, May 13, 2002, DOI 10.1074/jbc.M111777200

Orna Almog‡, D. T. Gallagher§¶, Jane E. Ladner§, Susan Strausberg§, Patrick Alexander§, Philip Bryan§, and Gary L. Gilliland§‖

From the ‡Department of Clinical Biochemistry, Faculty of Health Sciences, Ben-Gurion University, Beer-Sheva 84105, Israel and the §Center for Advanced Research in Biotechnology of the University of Maryland Biotechnology Institute and the National Institute of Standards and Technology, Rockville, Maryland 20850

The crystal structures of two thermally stabilized subtilisin BPN′ variants, S63 and S88, are reported here at 1.8 and 1.9 Å resolution, respectively. The micromolar affinity calcium binding site (site A) has been deleted (Δ75–83) in these variants, enabling the activity and thermostability measurements in chelating conditions. Each of the variants includes mutations known previously to increase the thermostability of calcium-independent subtilisin in addition to new stabilizing mutations. S63 has eight amino acid replacements: D41A, M50F, A73L, Q206W, Y217K, N218S, S221C, and Q271E. S63 has 75-fold greater stability than wild type subtilisin in chelating conditions (10 mM EDTA). The other variant, S88, has ten site-specific changes: Q2K, S3C, P5S, K43N, M50F, A73L, Q206C, Y217K, N218S, and Q271E. The two new cysteines form a disulfide bond, and S88 has 1000 times greater stability than wild type subtilisin in chelating conditions. Comparisons of the two new crystal structures (S63 in space group $P2_1$ with Å cell constants 41.2, 78.1, 36.7, and $\beta = 114.6°$ and S88 in space group $P2_12_12_1$ with cell constants 54.2, 60.4, and 82.7) with previous structures of subtilisin BPN′ reveal that the principal changes are in the N-terminal region. The structural bases of the stabilization effects of the new mutations Q2K, S3C, P5S, D41A, Q206C, and Q206W are generally apparent. The effects are attributed to the new disulfide cross-link and to improved hydrophobic packing, new hydrogen bonds, and other rearrangements in the N-terminal region.

The serine protease subtilisin (Sbt),[1] secreted by the soil bacterium *Bacillus amyloliquefaciens*, is one of the best studied proteases (1–5) and is widely used as a detergent additive (3). The use of Sbt in chelating ("water-softening") detergent conditions causes a loss of bound calcium from the high affinity site A and results in destabilization and loss of activity. However, the simple deletion of site A from Sbt by removing the 9-residue A site loop (Δ75–83) creates an enzyme that is fully active but with sharply decreased thermostability. Some restabilization of the deletion mutant was achieved by incorporating the previously identified stabilizing mutations M50F, N218S, Y217K, and Q271E to produce the variant S46 (6). Together, these mutations extend the activity half-life of Δ75–83 Sbt by ~10-fold (7). To provide the further stability increases needed to regain in calcium-independent Sbt, the stability of wild type, a program of crystal structure analysis and directed evolution methods, was then developed.

The crystal structure of the first Δ75–83 Sbt (1SUC) showed that large structural perturbations were confined to the region of the deletion (4). The principal changes involve the N-terminal amino acids 1–6, the 36–44 Ω-loop, the 63–85 α-helix, and the 202–219 β-ribbon.[2] Several residues in these regions were observed in 1SUC to be repositioned, to have increased thermal factors, or to be completely disordered (residues 1–3). This structural analysis suggested amino acid positions that might be targeted for random mutagenesis and selection to restore stability to the loop-deleted enzyme. The basic criterion for selecting sites for mutagenesis was to assume that amino acids, which interact with the calcium loop in native subtilisin, were no longer optimal in the loop-deleted variant. The stabilizing amino acids were identified at the following positions: residues 2, 3, and 5; residues 41 and 43 in the Ω-loop; residue 73 in the α-helix; and residue 206 in the β-ribbon. When stabilizing mutations are combined, the resulting Sbt mutants regain the stability of wild type Sbt but are no longer dependent on calcium for stability. These Sbts illustrate alternative solutions to the calcium-mediated stabilization that evolved in natural Sbts. Proteins are highly refined by natural selection to perform efficiently in their native environments. In this case, we have synthetically evolved Sbts to perform efficiently in a non-native environment containing metal chelators.

Here we report the crystal structures of the thermostable calcium-independent subtilisin variants, S63 and S88, and examine structure/stability effects at the mutation sites. These crystal structures are compared with three other high resolution crystal structures of subtilisin that differ in crystallization conditions and in crystal symmetry, *i.e.* 1SUP (wild type subtilisin inhibited with phenylmethylsulfonyl fluoride) (5) and

* The costs of publication of this article were defrayed in part by the payment of page charges. This article must therefore be hereby marked "*advertisement*" in accordance with 18 U.S.C. Section 1734 solely to indicate this fact.

The atomic coordinates and structure factors (code 1GNS and 1GNV) have been deposited in the Protein Data Bank, Research Collaboratory for Structural Bioinformatics, Rutgers University, New Brunswick, NJ (http://www.rcsb.org/).

¶ To whom correspondence may be addressed. Center for Advanced Research in Biotechnology, University of Maryland Biotechnology Institute and the Institute of Standards and Technology, 9600 Gudelsky Dr., Rockville, MD 20850. Tel.: 301-975-5726; Fax: 301-975-5449; E-mail: travis.gallagher@nist.gov.

‖ To whom correspondence may be addressed. Tel.: 301-738-6262; Fax: 301-738-6170; E-mail: gary.gilliland@nist.gov.

[1] The abbreviations used are: Sbt, subtilisin BPN′; 1SUC, crystal structure of the first Δ75–83 Sbt; 1SUP, wild type subtilisin; DFP, diisopropyl fluorophosphate; 1SUA, calcium-independent Sbt variant; PEG, polyethylene glycol; S63, subtilisin BPN′ with the mutations D41A, M50F, A73L, Δ75–83, Q206W, Y217K, N218S, S221C, and Q271E; S88, subtilisin BPN′ with the mutations Q2K, S3C, P5S, K43N, M50F, A73L, Δ75–83, Q206C, Y217K, N218S, and Q271E.

[2] The wild type numbering was kept for all of the subtilisin variants; thus 1SUC, 1SUA, S63, and S88 have no residues numbered 75–83.

TABLE I
Summary of crystallographic and refinement statistics for S63 and S88

	S63	S88
Space group	$P2_1$	$P2_12_12_1$
Unit cell		
a (Å)	41.2	54.2
b (Å)	78.1	60.4
c (Å)	36.7	82.7
β (°)	114.6	
Resolution (Å)	8.0–1.8	8.0–1.9
Reflection		
Observations	64,819	72,438
Unique possibilities	20,181	19,754
Unique measured ($I > 2\sigma$)	15,590 (77%)	17,067 (86%)
R_{sym}[a]	0.055	0.088
Least squares refinement		
Atom totals		
Protein	1891	1880
Inhibitor	Oxidized Cys	diisopropyl fluorophosphate
Solvent molecules	129	132
Crystallographic R-factor[b]	16.5	17.6
Root mean square deviation (Å)		
Bond distance	0.020	0.020
Bond angle	0.040	0.040

[a] $R_{sym} = \Sigma(I_{ij} - G_{ij}\langle I\rangle_j)/\Sigma|I_{ij}|$ where $G_{ij} = g_i + A_i s_j + B_i s_j^2$ and $s = \sin\theta/\lambda$; g, A and B are scaling parameters.
[b] $R = \Sigma_{hkl}||F_o| - |F_c||/\Sigma_{hkl}|F_o|$.

TABLE II
Stability effects of mutations

Region of protein	Site	Stabilizing replacement	Relative half-life[a]
N terminus	Gln-2	Lys	2.0
	Gln-2	Leu	1.8
	Ser-3	none (without 206C)	
	Ser-3	Cys (S–S bond with 206)	17.0[b]
	Val-4	none	
	Pro-5	Ser	1.2
	Pro-5	Ser (with 3–206 disulfide)	2.8[c]
36–44 Ω-loop	Pro-41	Ala	1.5
	Asp-43	Asn	1.2
63–85 α-helix	Ala-73	Leu	2.6
	Ala-74	none	
202–220 β-ribbon	Gln-206	Val	4.5
	Gln-206	Trp	4.0
	Gln-206	Ile	4.0
	Gln-206	Cys (S–S bond with 3)	17.0[b]
	Tyr-214	none	

[a] Increases in half-life are relative to the calcium-free prototype S46.
[b] Cysteine mutations at positions 3 and 206 are stabilizing as a disulfide bond.
[c] Stabilization observed for P5S mutation in the presence of the 3–206 disulfide.

1SUC and 1SUA (two previously reported calcium-independent subtilisins) (4, 6).

MATERIALS AND METHODS

Selection of Mutations, Cloning, and Expression—Ten residues that interacted with the site A loop in wild type Sbt were targeted for replacement in the deletion mutant S46. Initially, mutagenesis was performed on the S46 gene using oligonucleotides that were degenerate at one codon to identify the optimum amino acid at that position. Mutant clones were grown in microtiter dishes and screened for the retention of enzymatic activity at high temperature (for review see Ref. 6). The expression and purification were as described previously (9). Following single site mutagenesis and screening, some sites were re-screened in the context of favorable mutations, and synergistic effects were identified by dual-site mutagenesis and screening as described below. The overall process of mutagenesis, selection, and further mutagenesis that led to the S88 variant is described previously (6).

Activity Assays—The assays of peptidase activity were performed by monitoring the hydrolysis of sAAPF-pNA as described previously (10). The Sbt concentration was determined using 1 mg/ml = 1.12 at 280 nm (11). The activity measurements were conducted in 0.05 M Tris-HCl, pH 8.0, 0.05 M NaCl, and 0.01 M EDTA at 60 °C.

Determination of Inactivation Rates—The kinetics of thermal inactivation were determined. The enzyme at 1 μM concentration was dispensed in aliquots of 0.5 ml into 1-ml glass test tubes and covered with parafilm. The tubes were placed in a circulating water bath at the appropriate temperature. At each time point, a tube was removed and quickly transferred to an ice bath. A 10-μl aliquot was removed, and residual activity was assayed in 990 μl of 1 mM sAAPF-pNA, 0.1 M Tris-HCl, pH 8.0, and 0.1 M NaCl. The inactivation time course was followed over four half-lives.

Circular Dichroism—Thermal denaturation of inactive subtilisins was measured using a JASCO 720 spectropolarimeter. Protein samples at a concentration of 1.0 μM were monitored at 222 nm while heated at a uniform rate using a 1.0-cm path length jacketed cuvette. The temperature was increased with a circulating water bath interfaced with a NESLAB temperature programmer. The heating rate was 1 °C/min. Derivative melting curves were calculated using KaleidaGraph software for the Macintosh.

Crystallization—Crystallization used the hanging-drop vapor-diffusion method with siliconized coverslips and Linbro 24-well tissue culture plates. In these experiments, the droplets ranging in size from 10 to 20 μl were equilibrated with 1.0 ml of reservoir solution at 20 °C. Initial crystallization trials for both S63 and S88 employed a modification of the procedure reported by Drenth and Hol (12) that was used to grow crystals of 1SUC and other Sbt variants (4, 13). Crystallization droplets containing 10 mg/ml protein in 0.05 M glycine at pH 9.0 were suspended over a reservoir solution that contained 55% acetone and 0.05 M glycine, pH 9.0. Only the S63 variant crystallized under these conditions. In each droplet, 1–5 crystals appeared within a few days and grew to full size within 2 weeks with typical dimensions of 0.4 × 0.4 × 0.5 mm. The crystallization conditions for S63 are similar to the conditions found for 1SUC despite the 4 amino acid differences at sites 41, 73, 206, and 271.

Further trials employing the fast screen approach of Jancarik and Kim (14) were carried out for S88 using the Hampton Research crystal screen kit. The suspended droplets were prepared by mixing 5 μl of a protein solution containing 10 mg/ml S88 in 0.01 M HEPES-HCl and 0.02 M KCl at pH 7.5 and equal volumes of the reservoir solution. Small crystals appeared in droplets equilibrated against a solution containing 30% (w/v) PEG 4000, 0.2 M ammonium sulfate, and 0.1 M sodium acetate at pH 4.6. After refining the conditions, the final reservoir solution consisted of 23% (w/v) of PEG 4000, 0.2 M ammonium sulfate, and 0.1 M sodium acetate at pH 4.5. Using these conditions, 1–4 single crystals appeared in each droplet within 3 days and grew to 0.3 × 0.3 × 0.5 mm after two additional days.

X-ray Data Collection and Processing—The diffraction data from crystals of S63 and S88 mounted in thin-walled glass capillaries were collected at room temperature using a Bruker Hi-Star electronic area detector. The area detector was mounted on a Rigaku RU-200 HB generator operated at 40 kV and 60 mA. A graphite monochromator followed by a 0.5-mm collimator was used. The detector was positioned at 10 cm from the crystal, and 2θ was set to 26 and 24° intercepting data at 1.8 and 1.9 Å for S63 and S88, respectively. The diffraction data collected with the area detector were electronic images, each comprising a 0.2° oscillation counted for 3 min. The determination of unit cell parameters, crystal orientation, and the integration of reflection intensities were performed with the XENGEN program system (15). The crystallographic parameters and a summary of the data processing statistics for both S63 and S88 are given in Table I.

Structure Refinement—The structure of S63 was solved by direct replacement using 1SUC (4) as a starting model. The structure of S88 was also solved by direct replacement but, in this case, by using the variant 1SUA (8) as the starting model. In addition to the deletion, 1SUA has these eight mutations, K43N, M50F, A73L, Q206V, Y217K, N218S, S221C, and Q271E. As with the 1SUC crystal structure, 1SUA does not include the first three residues of the N terminus because of disorder. The starting model included the complete protein coordinates of 1SUA as well as 130 water molecules. The initial R-factor using this starting model was 0.29 for all data between 8.0 and 2.4 Å. At this stage, all of the side chains were changed to fit the correct sequence of S88, and all of the data between 8.0 and 1.9 Å were used. After several cycles of refinement and map fitting that included modification of the solvent

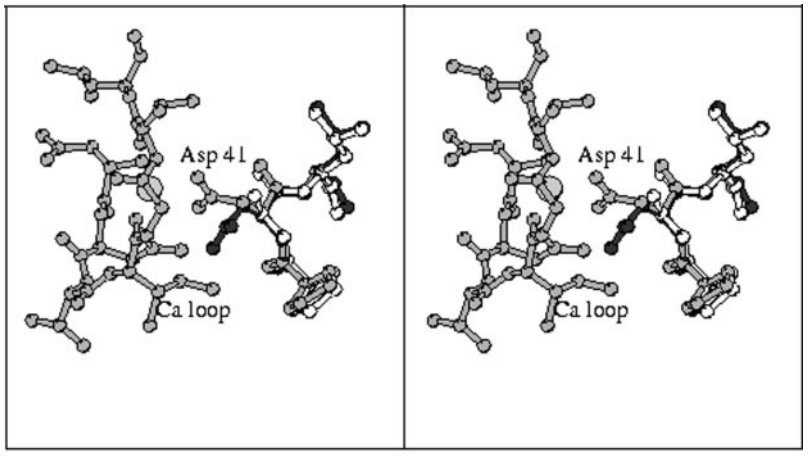

FIG. 1. **Stereo superposition of 1SUP (*gray*), 1SUC (*black*), and S63 (*white*) crystal structures in the region of residue 41.** The large *gray* sphere is the calcium ion that is coordinated by Asp-41 in the wild type **1SUP**. In the absence of the calcium loop, the side chain reorients (*black*). The structure is then stabilized by truncating the side chain (*white*).

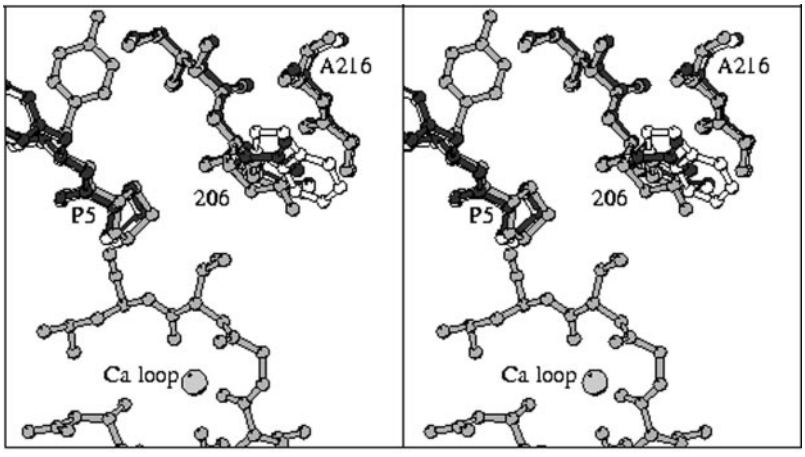

FIG. 2. **Stereo superposition of 1SUP (*gray*), 1SUC (*black*), and S63 (*white*) crystal structures showing the Q206W mutation.** The Q206 side chain adopts different conformations in its two structures. Tyr-6 is also visible in its two conformations.

TABLE III
Crystallization data for subtilisin BPN′ structures

	S63	S88	1SUC	1SUA	1SUP
Mutations	Δ75–83; D41A; M50F; A73L; Q206W; Y217K; N218S; S221C; Q271E	Q2K; S3C; P5S; Δ75–83; K43N; M50F; A73L; Q206C Y217K; N218S; S221-DFP Q271E	Δ75–83; M50F; Y217K; N218S; S221C	Δ75–83 K43N; M50F; A73L; Q206V Y217K; N218S; S221A; Q271E	
Active site	Oxidized Cys	DFP	Oxidized Cys	ALAL tetrapep.	PMS
Crystallization	55% acetone, 50 mM glycine, pH 9.0	23% PEG 4000, 0.2 M $(NH_4)_2SO_4$, 0.1 M $NaCH_3COO$, pH 4.5	55% acetone, 50 mM glycine, pH 9.0	1.25 M Li_2SO_4, 0.1 M HEPES, pH 7.0	1.5 M $(NH_4)_2SO_4$, 20 mM MES, pH 7.0
Space group	$P2_1$	$P2_12_12_1$	$P2_1$	$P2_12_12_1$	C2
Unit cell	a = 41.2 Å b = 78.1 Å c = 36.7 Å β = 115.0 °	a = 54.2 Å b = 60.4 Å c = 82.7 Å	a = 41.4 Å b = 78.7 Å c = 36.8 Å β = 115.0 °	a = 53.5 Å b = 60.3 Å c = 83.4 Å	a = 66.56 Å b = 54.15 Å c = 62.73 Å β = 91.87 °

structure, it was possible to fit the N-terminal residues to the electron density map.

The refinement of both crystal structures was carried out by the restrained parameter least squares procedure PROFFT (16–18). The program FRODO (19) was used to examine $2F_o - F_c$ and $F_o - F_c$ difference maps and omit maps to adjust the model, build the N-terminal region, and add water molecules. The statistics for the final model are given in Table I. The coordinates and structure factors for S63 and S88 have been deposited in the Protein Data Bank (20) as entries 1GNS for the S63 crystal structure and 1GNV for the S88 crystal structure.

Structure Analysis—An analysis of the final structures of S63 and S88 utilized PROCHECK (21). The superpositioning of these two molecules with other high resolution subtilisin structures was performed with the ALIGN program (22) using only the C-α atom positions of the polypeptide backbones. The two final structures of S63 and S88 were compared with three other high resolution subtilisin structures: 1SUP (wild type Sbt in the space group C2 at 1.6 Å resolution) (5), 1SUC (the first reported Δ75–83 Sbt structure at 2.0 Å resolution with mutations M50F, Δ75–84, Y217K, N218S, and S221C) (4), and 1SUA (a previously reported calcium-independent Sbt variant with mutations K43N, M50F, A73L, Δ75–84, Q206V, Y217K, N218S, and S221A at 2.1 Å resolution) (8).

RESULTS AND DISCUSSION

Structure of S63—The screening procedure identified stabilizing mutations at 7 of the 10 positions listed with stability effects in Table II. S63 has the active-site mutation S221C and the seven stabilizing mutations, D41A, M50F, A73L, Q206W, Y217K, N218S, and Q271E. Five of these substitutions have been described in previous structures; the two new mutations in S63 are D41A and Q206W. The final coordinates of S63 exclude residues 1–3 and the side chain of Val-4 because of disorder. The overall quality of the geometry of the final model is consistent with other Sbt structures determined at comparable resolution (Table I). The S63 cysteine residue is apparently oxidized as observed in the 1SUC structure.

D41A is shown in Fig. 1. In wild type Sbt, 1SUP, Asp-41

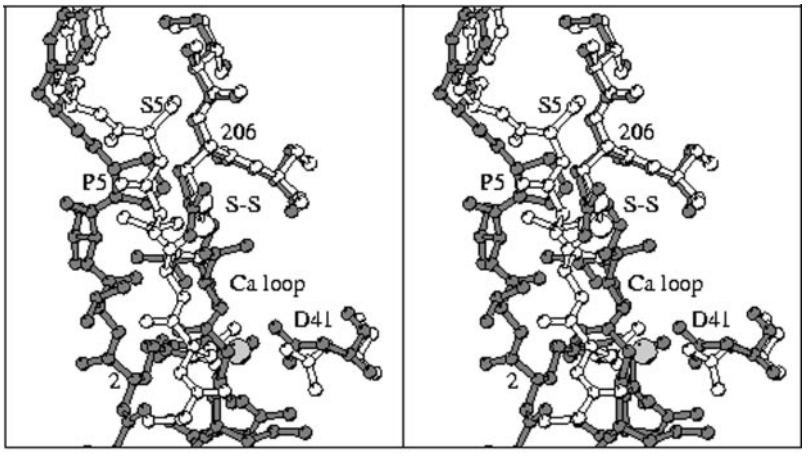

FIG. 3. **Electron density ($2F_o - F_c$ map contoured at 1σ) in the N-terminal region of S88 crystal structure including the disulfide, the new salt-link (Q2K-D41), and the N terminus.**

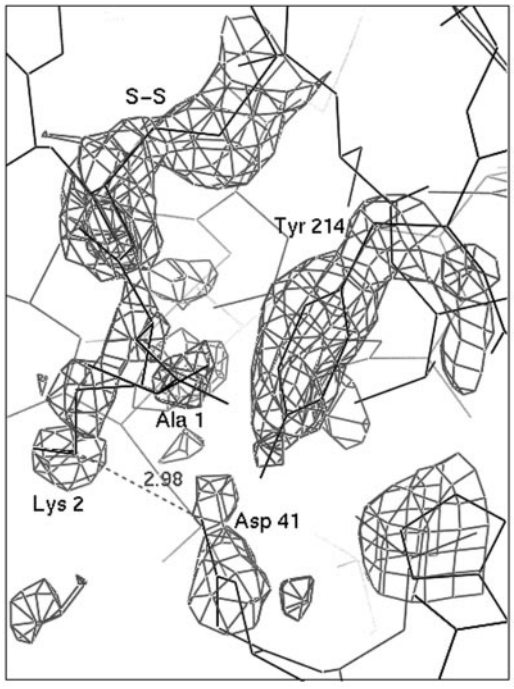

FIG. 4. **Stereo superposition of 1SUP (*gray*) and S88 (*white*) crystal structures in the region of the new disulfide linking Cys-3 and Cys-206.** Also evident are the general shift of the N terminus toward the space of the deleted loop, the Q2K mutation, and the conserved conformation of Tyr-6 between these two structures.

TABLE IV

Inactivation times and melting temperatures of subtilisin variants

Half-time was measured in 50 mM Tris-HCl, pH 8.0, 50 mM NaCl, and 10 mM EDTA at 60 °C using the active S221 variants on the left. For measurements of thermal unfolding, S34, S63, and S70 were modified to the inactive C221 versions S46, S59, and S67, respectively whereas the melting of wild type and S88 was carried out on the diisopropyl fluorophosphate-inactivated enzymes. All of the T_m measurements were carried out in 100 mM KPO_4, pH 7.0, at a scan rate of 1 °/min. Uncertainties are given in parentheses.

Subtilisin variant	$t_{½}$ (active version)	T_m
	min	*°C*
Wild type	0.2 (0.06)	65 (0.5)
S34/S46	2.1 (0.1)	69 (0.5)
S63/S59	15.0 (0.4)	71 (0.5)
S70/S67	16.5 (0.5)	71 (0.5)
S88	240.0 (4.0)	84 (0.5)

provides one coordination bond to the tightly bound calcium ion and also interacts through three hydrogen bonds with residues in the calcium-binding loop 75–83 (one hydrogen bond between the main chain carbonyl oxygen atom and the main chain amide N atom of Leu-75 (2.9 Å) and two hydrogen bonds between the side chain of Asp-41 and two other residues). The Asp-41 OD1 atom forms a hydrogen bond with the side chain ND2 of Asn-77 (2.8 Å), and Asp-41 OD2 atom forms a H-bond to the amide N of Val-81 (2.9 Å). The deletion of the calcium binding site (residues 75–83) eliminates those hydrogen bonds and leaves the side chain of Asp-41 unbound increasing the temperature factors of the side chain atoms. The D41A change apparently reduces the thermal motion at this site (lower B values) and increases the half-time of inactivation at 60 °C in S63 by 1.5-fold. No hydrogen bonds are seen for Ala-41 in the S63 crystal structure.

Q206W—Gln-206 was selected for mutagenesis because of its proximity to the N terminus that was found to be disordered by the removal of the high affinity calcium binding site. The rationale was that a different residue might form stronger interactions with the N terminus and hence increase the thermal stability by reducing the N-terminal mobility. The OE1 and NE2 atoms of the side chain of Gln-206 in the 1SUP crystal structure form hydrogen bonds with water molecules as well as two hydrogen bonds of the main chain to water molecules. However, in the crystal structure of 1SUC (only the hydrogen bonds found are between the main chain and water molecules), there are no hydrogen bonds involving the side chain of Gln-206. The same pattern was found in the S63 crystal structure. Two hydrogen bonds were found for Trp-206 in the crystal structure of S63; both involve the main chain 206. However, no interaction was found between the side chain of Trp-206 and the N terminus, which is still disordered in this crystal structure. The stabilizing effect of Q206W (increasing the half-life of Δ75–83 Sbt by 4-fold) probably involves its increased Van der Waals interaction (6, 23, 24) and reduced conformational freedom. The Gln side chain at this site has a variable conformation and above average temperature factors in 1SUP and 1SUC. The Trp side chain produces more extensive Van der Waals interaction by adopting a conformation with the indole packed against a peptide plane on the opposite strand of the β-ribbon (Fig. 2).

Structure of S88—S88 produced crystals isomorphous with the subtilisin variant 1SUA, although the crystallization conditions differ (Table III). The structure of S88 includes the inhibitor DFP bound to Ser-221. The N terminal could be fit from the electron density, but the density for residues Ala-1 and Lys-2 was relatively weak, and the occupancy for these two residues was modeled as 0.5. The electron density in the N-terminal region of S88 is shown in Fig. 3. S88 has four new mutations (Q2K, S3C, P5S, and Q206C), all are close to the N terminus.

Q2K—The Gln-2 side chain coordinates the calcium ion in wild type subtilisin. In the first Δ75–83 Sbt structure, 1SUC, residues 1–3 are disordered. The Q2K mutation doubles the half-time of inactivation of calcium-free Sbt relative to 1SUC (Table II). Lys-2 is observed to form two hydrogen bonds. The side chain amine forms a salt-link with Asp-41. This mimics the interaction of residue 41 to the calcium ion in wild type Sbt (see Figs. 3 and 4). The other hydrogen bond is between the main chain amide and a water molecule. These new bonds found in S88 are not seen in 1SUC and S63 in which the N terminus is disordered.

S3C and Q206C—Because computer graphics modeling indicated that positions 3 and 206 could potentially interact, the combinations of random mutations were screened at these two positions. This process resulted in a highly stabilizing disulfide with conformational angles $\chi_1 = -39°$, $\chi_2 = 180°$, $\chi_{SS} = -102°$, $\chi_{2'} = -104°$, and $\chi_{1'} = 75°$ (see Fig. 4). The electron density for the region is shown in Fig. 3. The 3–206 disulfide cross-link would not be able to form in any of the natural subtilisins, because the site A loop separates the N-terminal amino acids from the 202–219 β-ribbon. Therefore, the benefit of a 3–206 disulfide is novel to loop-deleted Sbts. The cross-link was found to increase the half-time of thermal inactivation 17-fold relative to 1SUC. Proteins reported previously to be stabilized because of introduced disulfides include subtilisin E (25), subtilisin BPN′ (26, 27), thermolysin-like protease (28), T4 lysozyme (29), and an Fv antibody fragment (30).

P5S—Serine was observed to be the best substitution for proline at position five in the S46 background (no disulfide) where this mutation resulted in only a 1.2-fold increase in half-life. Because of the potential interdependence of changes in this region, random mutations at positions 2, 5, and 41 were rescreened in the context of the 3–206 disulfide. Rescreening identified no new stabilizing mutations at positions 2 or 41 but showed the P5S change to result in significant stabilization. The P5S mutation in S88 subtilisin resulted in a 2.8-fold increase in half-life at 60 °C in 10 mM Tris-HCl, pH 8.0, 50 mM NaCl, and 10 mM EDTA (240 min compared with 85 min for Pro-5). Ser-5 forms five hydrogen bonds, two of them involving the hydroxyl to the main chain amide of residue 7 and to the buried side chain of His-226. Pro-5 in the 1SUC structure has only one hydrogen bond involving the main chain carbonyl. The new hydrogen bonds probably are primary factors in the increased thermal stability from the P5S mutation. The increased backbone flexibility of Ser may also play a part, although the φ- and ψ-angles of residue 5 are not significantly altered.

Enzyme Stability—The melting and thermal inactivation data for the wild type, 1SUP, S63, and S88 are presented in Table IV. To measure the activity of 1SUC and S63, cysteine 221 was changed back to serine 221, producing S46 and S59, respectively. The data were taken in chelating conditions (10 mM EDTA) at 60 °C. Although S88 and wild type have similar proteolytic activity at 25° without EDTA, S88 loses activity approximately 1000 times slower than wild type in EDTA at 60 °C. The $t_{1/2}$ for wild type is 0.2 min, and for S88, $t_{1/2}$ is 240 min. The $t_{1/2}$ for 1SUC is 2.1 min, and for S63, $t_{1/2}$ is 15 min. This means that in chelating conditions, S88 is more stable than the wild type, 1SUC, and S63. The same trend is found in the comparison of the melting temperatures of the wild type, 1SUC, S63, and S88.

Overall Comparison—The crystal structures of S63 and S88 were compared with each of the three other Sbts: 1) 1SUC, the first calcium-free Sbt; 2) 1SUP, wild type Sbt; and 3) 1SUA, calcium-free Sbt in the same crystal form as S88. The crystallization and mutation comparisons of five subtilisin variants are shown in Table III. The comparison of the five structures using the program ALIGN reveals that all of the structures are essentially the same but not in the region of the mutations. The root mean square deviation is below 0.3 Å for all of the comparisons. The superposition in Fig. 3 shows that the N terminus in the S88 crystal structure has moved toward the space created by the deletion of the calcium binding loop. The C-α positions of residues 1 and 2 have moved by 7.6 and 5.9 Å respectively. The point at which the path of the main chain diverges between the two structures is Gly-7 where the ψ-angle changed from 136° in 1SUP to 160° in S88. Interestingly, Tyr-6 is found in the same conformation in these two structures, but in 1SUC, 1SUA, and S63, the side chain of Tyr-6 adopts a different more exposed rotamer. Evidently the rotameric state of Tyr-6 is sensitive to the destabilization of the N terminus, and when the N terminus is retethered by the new disulfide, Tyr-6 returns to its wild type position.

S63 and S88 are two new variants of calcium-independent subtilisin, featuring several mutations selected for increased thermostability from random mutants. The crystal structures of S63 and S88 at high resolution have been determined, and the molecular structures of these two enzymes have been compared with three previous structures of Sbt. Despite the variations in sequence, chemical conditions, and crystal symmetry interactions, the structures are all similar but not in the N-terminal region adjacent to the site A deletion. S88 has a disulfide bond between the new cysteines at positions 3 and 206. This disulfide bond anchors the N terminus and contributes to the dramatic increase in thermostability in S88. In addition to the new disulfide bond, S88 includes several other mutations that combine to increase its thermostability relative to 1SUC by ~1000-fold in chelating conditions. The apparent mechanisms of stabilization include modulations of conformational flexibility, increases in Van der Waals interaction, and a salt-link and hydrogen bonds that stabilize the N terminus.

Acknowledgment—We thank Vincent Vilker for advice on the project and useful comments on this paper.

REFERENCES

1. Wright, C. S., Alden, R. A., and Kraut, J. (1969) *Nature* **221,** 235–242
2. Siezen, R. J., de Vos, W. M., Leunissen, J. A., and Dijkstra, B. W. (1991) *Protein Eng.* **4,** 719–737
3. Siezen, R. J., and Leunissen, J. A. (1997) *Protein Sci.* **6,** 501–523
4. Gallagher, T., Bryan, P., and Gilliland, G. L. (1993) *Proteins Struct. Funct. Genet.* **16,** 205–213
5. Gallagher, D. T., Oliver, J. D., Bott, R., Betzel, C., and Gilliland, G. L. (1996) *Acta Crystallogr. Sec. D* **52,** 1125–1135
6. Strausberg, S. L., Alexander, P. A., Gallagher, D. T., Gilliland, G. L., Barnett, B. L., and Bryan, P. N. (1995) *Bio/Technology* **13,** 669–673
7. Alexander, P. A., Ruan, B., Strausberg, S. L., and Bryan, P. N. (2001) *Biochemistry* **40,** 10640–10644
8. Almog, O., Gallagher, T., Tordova, M., Hoskins, J., Bryan, P., and Gilliland, G. L. (1998) *Proteins Struct. Funct. Genet.* **31,** 21–32
9. Bryan, P., Wang, L., Hoskins, J., Ruvinov, S., Strausberg, S., Alexander, P., Almog, O., Gilliland, G., and Gallagher, T. (1995) *Biochemistry* **34,** 10310–10318
10. DelMar, E., Largman, C., Brodrick, J., and Geokas, M. (1979) *Anal. Biochem.* **99,** 316–320
11. Pantoliano, M. W., Whitlow, M., Wood, J. F., Rollence, M. L., Finzel, B. C., Gilliland, G. L., Poulos, T. L., and Bryan, P. N. (1988) *Biochemistry* **27,** 8311–8317
12. Drenth, J., and Hol, W. G. (1967) *J. Mol. Biol.* **28,** 543–544
13. Bryan, P. N., Rollence, M. L., Pantoliano, M. W., Wood, J., Finzel, B. C., Gilliland, G. L., Howard, A. J., and Poulos, T. L. (1986) *Proteins Struct. Funct. Genet.* **1,** 326–334
14. Jancarik, J., and Kim, S.-H. (1991) *J. Appl. Crystallogr.* **24,** 409–411
15. Howard, A. J., Gilliland, G. L., Finzel, B. C., Poulos, T. L., Ohlendorf, D. H., Salemme, F. R. (1987) *J. Appl. Crystallogr.* **20,** 383–387
16. Hendrickson, W., and Konnert, J. (1980) in *Stereochemically Restrained Crystallographic Least Squares Refinement of Macromolecule Structures* (Diamond, R., Ramaseshan, S., Venktesan, K., eds) pp. 1301–1323, Indian Academy of Sciences, Bangalore, India
17. Finzel, B. C. (1987) *J. Appl. Crystallogr.* **20,** 53–55
18. Sheriff, S. (1987) *J. Appl. Crystallogr.* **20,** 55–57
19. Jones, T. A. (1978) *J. Appl. Crystallogr.* **11,** 268–272
20. Berman, H. M., Feng, Z., Gilliland, G. L., Bhat, T. N., Weissig, H., Shindyalov, I. N., and Bourne, P. E. (2000) *Nucleic Acids Res.* **28,** 235–242
21. Laskowski, R. A., Macarthur, M. W., Moss, D. S., and Thornton, J. M. (1993)

J. Appl. Crystallog. **26,** 283–291
22. Satow, Y., Cohen, G. H., Padlan, E. A., and Davies, D. R. (1986) *J. Mol. Biol.* **190,** 593–604
23. Yutani, K., Ogasahara, K., Tsujita, T., and Sugino, Y. (1987) *Proc. Natl. Acad. Sci. U. S. A.* **84,** 4441–4444
24. Eijsink, V. G., Dijkstra, B. W., Vriend, G., van der Zee, J. R., Veltman, O. R., van der Vinne, B., Vandenburg, B., Kempe, S., and Venema, G. (1992) *Protein Eng.* **5,** 421–426
25. Takagi, H., Takahashi, T., Momose, H., Inouye, M., Maeda, Y., Matsuzawa, H., and Ohta, T. (1990) *J. Biol. Chem.* **265,** 6874–6878
26. Mitchinson, C., and Wells, J. A. (1989) *Biochemistry* **28,** 4807–4815
27. Stausberg, S., Alexander, P. A., Wang, L., Gallagher, T., Gilliland, G. L., and Bryan, P. N. (1993) *Biochemistry* **32,** 10371–10377
28. Mansfeld, J., Vriend, G., Dijkstra, B. W., Veltman, O. R., Vandenburg, B., Venema, G., Ulbrich-Hofmann, R., and Eijsink, V. G. H. (1997) *J. Biol. Chem.* **272,** 11152–11156
29. Matsumura, M., Becktel, W. J., Levitt, M., and Matthews, B. W. (1989) *Proc. Natl. Acad. Sci. U. S. A.* **86,** 6562–6566
30. Almog, O., Benhar, I., Vasmatzis, G., Tordova, M., Lee, B., Pastan, I., and Gilliland, G. L. (1998) *Proteins* **31,** 128–138